

Supplementary Online Material

This Supplementary Online Material (SOM) consists of five sections: S.1 Parameter descriptions and estimation; S.2 Model derivation; S.3 Threshold conditions for population growth; S.4 Numerical methods; and S.5 The follow-up treatment window.

S.1 Parameter descriptions and estimation

Descriptions of all parameters are provided in Table S.1. The model (equations (1) and (2) in the main text) does not explicitly consider inflow and outflow of larval stages from the salmon netpens due to ocean currents, but we note that outflow likely exceeds inflow, such that the net effect is loss of larval lice from the salmon netpens. We assume that larvae that enter and leave the netpens have identical levels of development, such that larval net flow can be understood as being incorporated into two parameters: the mortality/loss rate of nauplii, $\mu_P(t)$, is considered to incorporate the net outflow of nauplii, such that if ocean currents are strong then $\mu_P(t)$ is larger, and the per fish attachment rate of copepodids, ι , is considered to incorporate the net outflow of copepodids, such that if ocean currents are strong, then ι is smaller. This approach to modelling larval flow is oversimplistic, but a more realistic formulation would require a substantial increase in model complexity, additional data, and it is not clear that this additional realism is necessary for our study.

Temperature and salinity are variable between sites, but the functions that describe the dependence of the model parameters on temperature, T , and salinity (measured in practical salinity units, psu), S , are the same across sites. The equations for life history parameters as a function of temperature and salinity were estimated by fitting curves to the laboratory results and the assumed functional forms were based on previous studies (Stien et al., 2005; Rittenhouse et al., 2016; Samsing et al., 2016).

Our model parameterization focuses on the *Lepeophtheirus salmonis* species of salmon lice. *L. salmonis* consists of two subspecies: *salmonis*, found in the Atlantic ocean, and *oncorhynchi*, found in the Pacific Ocean. These subspecies are genetically different, although, less so than different species (Skern-Mauritzen et al., 2014), and are capable of reproducing, but do not do so due to geographic barriers. It is not known whether these genetic differences at the subspecies level affect life history parameters (Elmoslemany et al., 2015), but a prior study (Stien et al., 2005) aggregates data from both subspecies. It is not possible to fully parameterize our model for one subspecies because not all relationships have been studied for both subspecies. Laboratory data that used the *salmonis* (black symbols) and *oncorhynchi* (blue symbols) subspecies are indicated in Figure S.1 and data from both subspecies of *L. salmonis* were combined to estimate the statistical fits.

Laboratory data for *Caligus rogercresseyi*, the salmon louse species that is dominant in Chile (Costello, 2006), are shown in green in Figure S.1. The *C. rogercresseyi* data was not considered for the statistical fits, but is shown for comparison. *C. rogercresseyi* do not have a pre-adult stage, but our modelling framework (equations (1) and (2)) aggregates both the chalimi and pre-adult stages into the attached, non-reproductive $C(t)$ -stage, and so our model is an appropriate framework for *C. rogercresseyi*.

For all parameters related to egg hatching, $v(T, S)$, $\eta(T)$, and $\epsilon(T)$, the data from Samsing et al. (2016 - crosses) may be most reliable since adult female lice were allowed to remain attached to their host salmonid during this study, whereas adult female salmon lice were removed from their host fish and transported to a laboratory for all other studies (Johnson and Albright, 1991; Boxaspen and Naess, 2000; Heutch et al., 2000; Bravo, 2010).

Table S.1 Description of model parameters.

Parameters	Description	Dimensions
ι	Attachment rate	time ⁻¹ number ⁻¹
f	Number of fish per farm	number
$\eta(t)$	Eggs per clutch	unitless
$\epsilon(t)$	Egg string production rate	time ⁻¹
$v(t)$	Proportion of eggs that produce viable nauplii	unitless
$\mu_P(t)$	Mortality rate of nauplii	time ⁻¹
$\mu_I(t)$	Net loss rate of copepodids	time ⁻¹
$\mu_C(t)$	Mortality rate of chalimi and pre-adults	time ⁻¹
$\mu_A(t)$	Mortality rate of adult females	time ⁻¹
$\gamma_P(t)$	The maturation rate of nauplii	time ⁻¹
$\gamma_C(t)$	The maturation rate of chalimi and pre-adults	time ⁻¹
$\tau_P(t)$	The time taken to complete the nauplii stage for nauplii that mature to the copepodid stage at time, t	time
$\tau_C(t)$	The time taken to complete the chalimi and pre-adult stages for louse that mature to the adult female stage at time, t	time

The viability of salmon lice eggs depends on both temperature and salinity, and is,

$$v(T, S) = \begin{cases} -2.2579 + 0.46 \log(T) + 0.64 \log(S) & \text{if } 0 \leq v \leq 1, \\ 1 & \text{if } v > 1, \\ 0 & \text{if } v < 0. \end{cases} \quad (\text{S.1})$$

The data that describes the effect of temperature is from *L. salmonis salmonis* (Figure S.1a), while the data describing the effect of salinity is from *L. salmonis oncorhynchi* (Figure S.1b). Published data are insufficient to determine a temperature by salinity interaction since only fixed salinity is considered for a range of temperatures (Samsing et al., 2016), and fixed temperature is considered for a range of salinity (Johnson and Albright, 1991).

The number of eggs per string is,

$$\eta(T) = \exp(5.6 - 0.43 \log(T/10) - 0.78 \log(T/10)^2), \quad (\text{S.2})$$

which is the fit described by Samsing et al. (2016) for *L. salmonis salmonis* (Figure S.1c). Data from Boxaspen and Naess (2000 - open squares) were excluded as they were not consistent with Samsing et al. (2016 - crosses). Bravo (2010) reports 31 eggs per string for *C. rogercresseyi* during an experiment where temperatures ranged from 10 - 18.5°C, and explains that this lower number of eggs per string may be because *C. rogercresseyi* is three times smaller than *L. salmonis*. Costello (2006) states that the number of eggs per string ranges from 100 to 1000 and depends on the time of year, host species, and louse species and size, also stating that 500 eggs per female louse is likely an underestimate for louse attached to farmed salmonids.

The rate of egg string production is,

$$\epsilon(T) = \min(\exp(-1.86 + 1.30 \log(T/10)), 1/45.1), \quad (\text{S.3})$$

where the minimum is taken to prevent extrapolation beyond the minimum temperature observed experimentally. The fit is based on data which are a mix of the two *L. salmonis* subspecies, but these data from different subspecies agree quite closely (Figure S.1d, blue and black symbols). Data for *C. rogercresseyi* (Figure S.1d, green squares containing an ×, Montory et al. 2018) was not considered for the model fit, but shows that egg strings are produced more quickly for *C. rogercresseyi* at 5-10°C as compared to *L. salmonis*.

The maturation rate of nauplii to copepodids is,

$$\gamma_P(T) = \min(\exp(-1.22 + 1.38 \log(T/10)), 1/23.5). \quad (\text{S.4})$$

The minimum is taken to prevent extrapolation below 2°C, the lowest temperature for which nauplii maturation experiments were performed. The function $\gamma_P(T)$ was also estimated in Stien et al. (2005), however, the fit described in equation (S.4) also considers more recent data collected by Samsing et al. (2016, Figure S.1e, crosses). While some data for the *oncorhynchi* subspecies (Figure S.1e, blue squares, Johnson and Albright 1991) are included in the model fit, these data are consistent with the data for the *salmonis* subspecies (Figure S.1e, black symbols). The maturation rate of nauplii for *C. rogercresseyi* (Figure S.1e, green squares with an \times , Montory et al. 2018) is also consistent with *L. salmonis* (black symbols).

For the rate of maturation from chalimus to adult female, we use the fitted values of Stien et al. (2005),

$$\gamma_C(T) = \min(0.00022(T + 1.94)^2, 0.0217), \quad (\text{S.5})$$

where the minimum is taken to prevent extrapolation below 8°C, the lowest temperature for which chalimi maturation rates were measured (Figure 4c in Stien et al. 2005; Figure S.1e in this SOM). The data measuring the maturation rate of chalimi for *C. rogercresseyi* (Figure S.1e, green circles with a +, Gonzalez and Carvajal 2003) are consistent with the fitted relationship from Figure 4c in Stien et al. 2005, which relies on data from laboratory experiments that used *L. salmonis salmonis*.

The mortality rates of nauplii, copepodid, chalimus and adults are assumed to be a function of salinity. For nauplii,

$$\mu_P(S) = \max(2.16, \exp(13.64 - 0.515S)), \quad (\text{S.6})$$

(see Figure S.1f). This function assumes that nauplii survive half a day at low salinities and becomes very large for high salinities consistent with the observation that all nauplii survived at 34 psu (Samsing et al., 2016). Samsing et al.’s observation is from *L. salmonis salmonis*, but all other observations are for the *oncorhynchi* subspecies.

For copepodids there is some evidence of a relationship between temperature and mortality in *C. rogercresseyi* (Figure S.1g, Montory et al. 2018). These data are shown to comprehensively report all data we assembled to parameterize our model, but our model assumes no temperature-mortality relationship because no studies for *L. salmonis* found this relationship.

For copepodids, the salinity-mortality relationship that we assume is,

$$\mu_I(S) = \exp(-0.0232 - 0.059S), \quad (\text{S.7})$$

(see Figure S.1h). These data are a mix of the two *L. salmonis* subspecies. The data from Bricknell et al. (2006, open diamonds) was excluded from the fit because these data were not consistent with Tucker et al. (2002, solid circles) and Samsing et al. (2016, crosses) at 32 psu. For lower salinities, other than Bricknell et al. (2006, open diamonds) which was excluded, the only available data is from Johnson and Albright (1991, blue solid square) and these data are for the *oncorhynchi* subspecies. For *C. rogercresseyi*, data from Montory et al. (2018) shows that mortality rates are low (Figure S.1h, green square with an \times) relative to *L. salmonis* at 34 psu.

Based on Connors et al. 2008 (Figure S.1h, blue inverted triangles), the relationship between salinity and the mortality rate for the parasitic salmon lice stages is,

$$\mu_C(S) = \mu_A(S) = \min(\exp(-4.12 - 0.124S), 24/1963). \quad (\text{S.8})$$

The experiments of Connors et al. (2008) did not distinguish between the mortality rates of chalimi and adult salmon lice and so we set $\mu_C(S) = \mu_A(S)$. In addition, the highest salinity considered by Connors et al. (2008)

was 28 psu at which salmon lice survived 1963 hours: the salinity in salmon aquaculture pens at our sites may approach 35 psu, and to prevent extrapolation of the mortality function beyond what was observed we set a lower bound on the per capita mortality rate at 24/1963 lice per day. The estimates of $\mu_A(S)$ for *C. rogercresseyi* (Figure S.1h, green squares containing a triangle) are from fitting an exponential decay function to the adult survival data in Table 1 of Bravo et al. (2008), however, these data are for adult sea lice removed from a host fish with subsequent survival monitored for 24 hours, while Connors et al.’s methodology considers parasitic *L. salmonis oncorhynchi* attached to pink *Oncorhynchus gorbuscha* and chum *O. keta* salmon monitored for > 1963 hours. Therefore, the Connors et al. (2008) data was considered more accurate. Nonetheless, *Caligus elongatus* are more sensitive to salinity than either *L. salmonis* or *C. rogercresseyi* as Landsberg et al. (1991) found that after 20 minutes at 8.2 psu none of the *C. elongatus* which had been attached to red drum (*Sciaenops ocellatus*) were still alive. In contrast, after 30 mins at 10 psu, 95-100% of *C. rogercresseyi* were still alive, with this percentage dropping to 15-45% after 24 hours (Bravo et al., 2008). Furthermore, the experiments of Connors et al. (2008) suggest that at 8.2 psu, 50% of adult *L. salmonis* will still be alive after 7 days.

Laboratory experiments have investigated the relationship between temperature and the copepodid attachment rate, ι , however no clear relationship was demonstrated (Figure S.1j). Bricknell et al. (2006) reports a relationship between salinity and the number of copepodids attached to salmon, however, the data describing natural mortality during this experiment are insufficient to allow us to estimate ι . We also expect that ocean currents may have a strong effect on copepodid attachment rates and these effects may be more important than temperature and salinity.

Only the BCB site contained sufficient data to estimate the number of fish on a farm, f , and the copepodid attachment rate, ι . Our mathematical model assumes a constant number of fish and no chemotherapeutic treatments and the BCB site satisfies these assumptions between March 3, 2003 to January 4, 2004. To estimate f , we calculated the mean number of fish on the BCB farm during the aforementioned period (506,737). During this same time period, we used data describing the number of *L. salmonis oncorhynchi* chalimi, pre-adults, and adult females, and performed maximum likelihood assuming a normal distribution of error to estimate the attachment rate with seasonality, $\iota = 2.1 \times 10^{-9}$ (Figure S.1j,k, solid line), and ignoring seasonality, ι as 2.4×10^{-9} (Figure S.1j,k, dashed line), by considering only the average temperature ($a = 8.3^\circ\text{C}$).

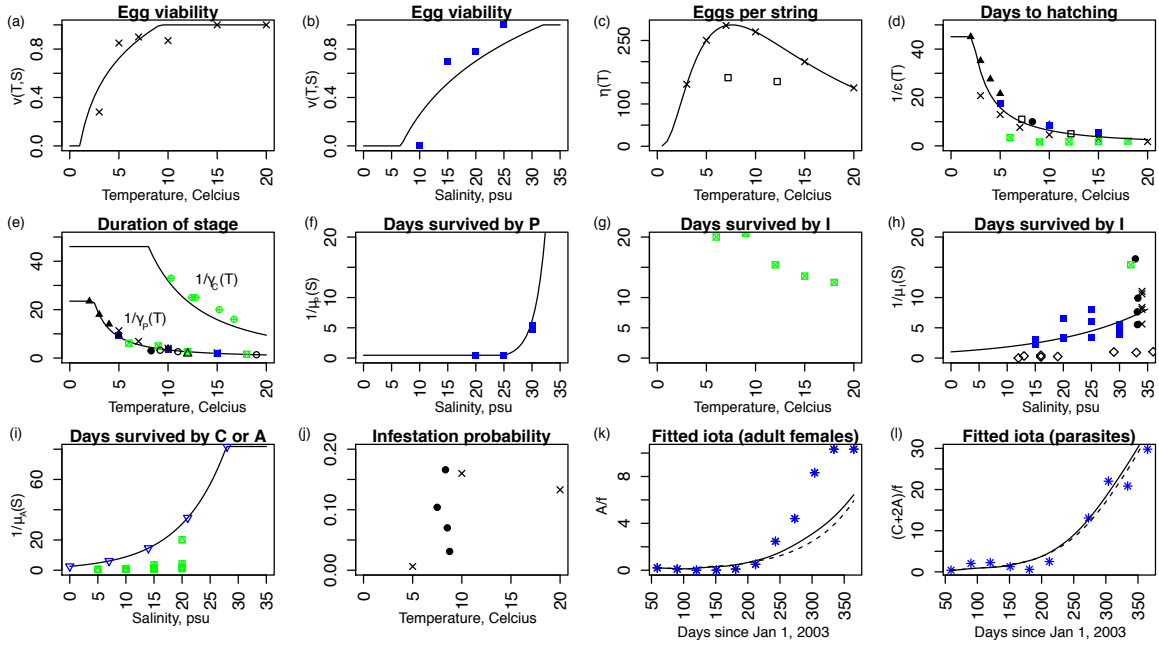


Fig. S.1 Published laboratory studies describe the relationship between life history parameters and temperature and salinity. We fitted functions (lines) to data from published laboratory studies (symbols) with *Lepeophtheirus salmonis salmonis* (black) and *L. salmonis oncorhynchi* (blue). Data from published laboratory studies with *Caligus rogercresseyi* are shown with green symbols: these data are for comparison and were not used for model fits. Black symbols (*L. salmonis salmonis*): Samsing et al. 2016 - crosses; Heutch et al. 2000 - open squares; Boxaspen and Naess 2000 - solid triangles; Tucker 2002 - solid circles; Johanessen 1978 - open circles; Wootten et al. 1982 - open triangles; and Bricknell et al. 2006 - open diamonds. Blue symbols (*L. salmonis oncorhynchi*): Johnson and Albright 1991 - solid squares; Connors et al. 2008 - open inverted triangles; and Marty et al. 2010 - astericks. Green symbols: Montory et al. 2018 - square with \times ; Bravo et al. 2008 - square with triangle; and Gonzalez and Carvajal 2003 - circle with $+$. Full details of the model parameterization and the equations are found in Section S.1.

S.1.1 Local adaptation

In Table S.2, we list all the data sources for the parameterization of each of the functions equations (S.1) - (S.8), as well as the origin of the salmon lice and the approximate year of the experiment. This is pertinent information to assess any bias that could arise due to local adaptation since our analyses apply these parameter estimates worldwide. We investigate local adaptation directly for the nauplius maturation rate, $\gamma_P(T)$, because salmon lice of varied geographic origins contribute to this parameter estimate. In Figure S.2, we consider the source of origin of the *L. salmonis* in relation to local temperatures and the fitted $\gamma_P(T)$ curve. We consider salmon lice ‘adapted’ if the temperature of the laboratory experiment (Figure S.2, the horizontal position of the symbols) is within the temperature range for the region of origin for the salmon lice (Figure S.2, the horizontal range of the bolded portion of the curve), and visa versa for ‘not adapted’. Firstly, we note that adapted and not adapted salmon lice have recorded near identical number of days in the nauplius stage prior to maturation, for example, in British Columbia salmon lice are not adapted at 15°C, but mature after the same number of days as lice from Norway which are adapted at this temperature. Secondly, the experiments are not performed at extreme temperatures beyond the natural ranges that the salmon lice are adapted to: only lice originating from Norway have been exposed to very cold temperatures during experiments, and in our model, only populations from Norway (and Atlantic Canada where source populations would also be adapted to cold temperatures) are simulated at these low temperatures. Therefore, the data used to parameterize $\gamma_P(T)$ do not suggest that local adaptation is biasing our results.

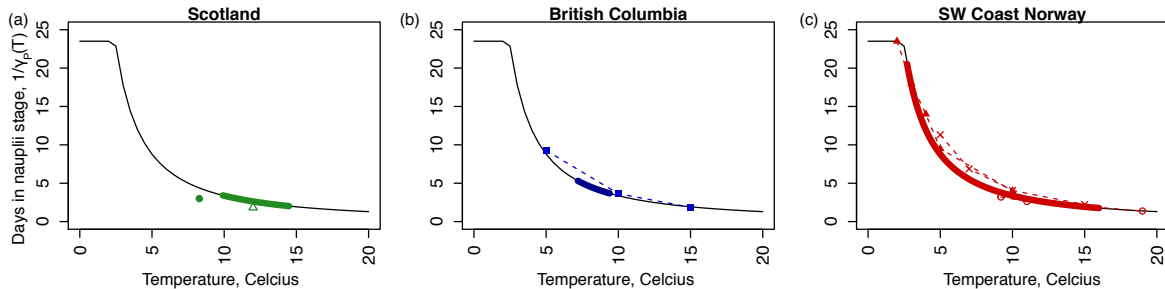


Fig. S.2 Local adaptation in *L. salmonis* does not invalidate our parameter estimates. We consider the origin of *L. salmonis* in relation to experimental data describing the number of days in the nauplii stage until maturation. We consider laboratory experiments where *L. salmonis* originate from a) Scotland (green symbols), b) the east coast of Vancouver Island, British Columbia (blue symbols), and c) Southwest Norway (green symbols). The temperatures for these experiments is compared to the range of sea surface temperatures from a nearby region (bold coloured portion of the curve), which corresponds to: a) Northern Ireland (IM4), b) Broughton Archipelago, British Columbia (BCB), and c) Lista, Norway (NLI). The fitted $1/\gamma_P(T)$ curve is shown in black. The experiments are performed at temperatures close to the local temperatures experienced by the salmon lice. Salmon lice exposed to temperatures outside the range they are adapted to record similar values to adapted salmon lice exposed to the same temperatures. The symbols are green: Tucker 2002 - solid circles and Wootten et al. 1982 - open triangles; blue: Johnson and Albright 1991 - solid squares; and red: Samsing et al. 2016 - crosses; Johannesssen 1978 - open circles and Boxaspen and Naess 2000 - solid triangles.

Table S.2 The source of all data used to parameterize functions of temperature and salinity. All data are for *Lepeophtheirus salmonis* for the subspecies *salmonis* (no underline) and *oncorhynchi* (underline). Definitions of the parameter symbols are provided in Table S.1. Origin describes the place of origin for the salmon lice used for the experiments. The year is the publication year, unless the year of the experiment is specified (denoted with *). Range is the range of temperature or salinity values over which measurements are taken. For Boxaspen and Naess (2000), the origin of the salmon lice was not stated, but the text suggested the origin was Norway (denoted with **).

Parameter	Origin	Year	Range (°C or psu)	Reference
$v(T)$	SW coast Norway	2015*	[3,20]	Samsing et al. (2016)
$\eta(T)$	SW coast Norway	2015*	[3,20]	Samsing et al. (2016)
$\epsilon(T)$	<u>E coast Vancouver Island, Canada</u>	1991	[5,15]	Johnson and Albright (1991)
	SW coast Norway	2015*	[3,20]	Samsing et al. (2016)
	Norway?	2000	[2,10]	Boxaspen and Naess (2000)
	W coast Norway	2002	[7.2,12.2]	Heutch et al. (2000)
	W coast Scotland	2002	8.3	Tucker (2002)
$\gamma_P(T)$	<u>E coast Vancouver Island, Canada</u>	1991	[5,15]	Johnson and Albright (1991)
	SW coast Norway	2015*	[5,15]	Samsing et al. (2016)
	Norway**	2000	[2,10]	Boxaspen and Naess (2000)
	W coast Scotland	2002	8.3	Tucker (2002)
	Norway/sea water aquaria at 9 and 11°C	1978	[9.2,19]	Johanessen (1978)
	Scotland?	1982	12°C	Wootten et al. (1982)
$\gamma_C(T)$	W coast Norway	1996	[9,10]	Grimnes and Jakobsen (1996)
	N Norway	1997*	9.7	Bjorn et al. (1998)
	Reared at 7.5°C/W coast Norway?	2000	7-10 variable	Finstad et al. (2001)
	W coast Scotland	2002	8.3	Tucker (2002)
$v(S)$	<u>E coast Vancouver Island, Canada</u>	1991	[10,25]	Johnson and Albright (1991)
$\mu_P(S)$	<u>E coast Vancouver Island, Canada</u>	1991	[20,30]	Johnson and Albright (1991)
	SW coast Norway	2015*	34	Samsing et al. (2016)
$\mu_I(S)$	<u>E coast Vancouver Island, Canada</u>	1991	[15,30]	Johnson and Albright (1991)
	SW coast Norway	2015*	34	Samsing et al. (2016)
	W coast Scotland	2002	[32.8,33.3]	Tucker (2002)
$\mu_C(S)$	<u>Broughton Archipelago, Canada</u>	2006*	[0,28]	Connors et al. (2008)

S.1.2 Temperature and salinity

We assume that temperature and salinity are seasonal and described by,

$$\begin{aligned} T(t) &= a + b_1 \sin(2\pi t/365) + b_2 \cos(2\pi t/365), \\ S(t) &= c + d_1 \sin(2\pi t/365) + d_2 \cos(2\pi t/365), \end{aligned} \tag{S.9}$$

where a is the mean sea surface temperature in degrees Celcius ($^{\circ}C$), c , is the mean salinity in psu, b_1 and b_2 affect the magnitude and timing of annual temperature changes, and d_1 and d_2 affect the magnitude and timing of annual salinity changes. For the BCB and NL sites, the salinity data was not seasonal since fitting the d_1 and d_2 coefficients did not improve the proportion of the variance explained (R^2) by more than 0.02, and so d_1 and d_2 were set to zero at these sites. For all the sites in Canada, both temperature and salinity data were available, but for the sites in Chile, Ireland, and Norway only temperature data was available; here we assume a constant salinity of 31 psu, which was the mean salinity for all sites with available data, but excluding the NL site where salinity was very low. To facilitate comparisons with the Northern Hemisphere sites, the temperate data from Region X, Chile was shifted by 182.5 days (Figure 1).

Temperature and salinity data as shown in Figure 1 were compiled from several sources as described below.

CH: Finfish farm near Puerto Montt, Region X, Chile Data consists of sea surface temperatures recorded from June 2000 to February 2001 (Bravo, 2003). This was the only southern hemisphere site and data was shifted by 182.5 days to enable comparisons with other sites. No salinity was available for this region, so our analyses assume a constant salinity of 31 psu, which is the average salinity reported for the BCB, BCC, BCV, NS and NB sites.

IM3: Weather buoy west of Ireland Mean monthly temperature recorded from 2003-2013 at the M3 weather buoy west of Ireland (Dabrowski et al., 2016). No salinity data was available for this region, so our analyses assume a constant salinity of 31 psu.

IM4: Weather buoy west of Ireland Mean monthly temperature recorded from 2003-2013 at the M4 weather buoy west of Ireland (Dabrowski et al., 2016). No salinity was available for this region, so our analyses assume a constant salinity of 31 psu.

BCB: Finfish farm in the Broughton Archipelago, British Columbia, Canada Temperature and salinity data is from farm 24 in Marty et al. (2010) collected Jan 1, 2001 - Nov 1, 2007. Salinity at this site is consistent with an ‘oceanic’ site as described by Groner et al. (2016).

BCC: Lighthouse on the Central Coast of British Columbia, Canada Mean monthly temperature and salinity (1954-2011) recorded at the McInnes Island lighthouse. Data is from Figure 3 in Brewer-Dalton et al. (2015).

BCV: Lighthouses on the west coast of Vancouver Island, BC. Mean monthly temperature and salinity (1935-2012) recorded at the Amphitrite Point and Kains Island lighthouses. Data is from Figure 2 in Brewer-Dalton et al. (2015).

NB: Hydrographic station in the mouth of the Bay of Fundy, NB. Mean monthly temperature and salinity (1971-2000) recorded at the Prince 5 hydrographic station. Data is from Figures 25 and 28 in Brewer-Dalton et al. (2015).

NS: Hydrographic station located off Halifax, Nova Scotia, Canada. Mean monthly temperature and salinity (1971-2000) recorded at the Station 2 hydrographic station located off Halifax, Nova Scotia. Data is from Figures 25 and 28 in Brewer-Dalton et al. (2015).

NL: Hermitage Bay-Bay d’Espoir, Newfoundland, Canada. Mean monthly temperature is from Figure 8 of Department of Fisheries and Oceans (2016). Monthly salinity was provided by the Department of Fisheries and Oceans (see Acknowledgements), but similar data is shown in Figure 18 in Brewer-Dalton et al. (2015). Salinity data with no associated depth was removed and only measurements taken between for 0-5m were included in the analysis. These salinity data were collected between 1994 and 2009.

NIN: Meterological station in Ingøy, Norway. Mean temperature measured every 14 days at a meterological station since 1942. Data is from Figure 1 in Samsing et al. (2016). No salinity data was available for this region, so our analyses assume a constant salinity of 31 psu.

NLI: Meterological station in Lista, Norway. Mean temperature measured every 14 days at a meterological station since 1942. Data is from Figure 1 in Samsing et al. (2016). No salinity data was available for this region, so our analyses assume a constant salinity of 31 psu.

Table S.3 Site specific temperature and salinity parameter estimates. Parameters are described in equations (S.9): notably, a is the mean temperature and c is the mean salinity. Where the inclusion of d_1 and d_2 improves R^2 by less than 0.02, this is indicated by * and parentheses indicate that these values were set to zero for the analyses. Where parameters cannot be calculated due to unavailable data this is indicated by -.

Location	a	b_1	b_2	c	d_1	d_2
CH	12.0	-0.9	-1.2	-	-	-
IM3	13.0	-1.5	-2.4	-	-	-
IM4	12.2	-1.1	-2.0	-	-	-
BCB	8.3	-0.8	-0.7	31.7	(0.7)*	(-0.4)*
BCC	9.7	-2.1	-2.8	30.2	0.3	-0.2
BCV	10.4	-1.8	-2.2	29.9	-0.5	-1.2
NS	6.7	-6.0	-2.3	30.8	0.4	-0.1
NB	6.7	-4.9	-3.8	31.9	-0.6	0.5
NL	6.0	-4.8	-2.5	20.0	(-1.9)*	(-7.3)*
NIN	6.5	-1.9	-1.8	-	-	-
NLI	9.3	-4.1	-5.3	-	-	-

S.2 Model derivation

Here we derive the mathematical model describing salmon lice dynamics (equations (1) and (2)). This derivation is provided in Rittenhouse et al. (2016), but in this section we provide some additional details, which will be useful for some readers. One minor difference between our model and that of Rittenhouse et al. (2016) is that our model has the number of eggs per string, $\eta(t)$, and the egg string production rate, $\epsilon(t)$ depend on time.

Our mathematical model for salmon lice population dynamics incorporates a temperature-dependent maturation delay and salinity-dependent mortality rates. We note that temperature and salinity are time-dependent. Let $M_P(t)$ be the maturation rate of nauplii, and $M_C(t)$ be the maturation rate of chalimi/pre-adults. Assuming

a 1:1 sex ratio, $\frac{1}{2}M_C(t)$ is the maturation rate of chalimi/pre-adults to the adult female stage. Then,

$$\begin{aligned}
\frac{dP(t)}{dt} &= \eta(t)\epsilon(t)v(t)A(t) - M_P(t) - \mu_P(t)P(t), \\
\frac{dI(t)}{dt} &= M_P(t) - \iota f I(t) - \mu_I(t)I(t), \\
\frac{dC(t)}{dt} &= \iota f I(t) - M_C(t) - \mu_C(t)C(t), \\
\frac{dA(t)}{dt} &= \frac{1}{2}M_C(t) - \mu_A(t)A(t),
\end{aligned} \tag{S.10}$$

where the variables $P(t)$, $I(t)$, $C(t)$ and $A(t)$ are each salmon lice stage. All parameters are defined in Table S.1. To derive a model with time-delayed maturation after a threshold level of development is completed, we follow the model derived in Nisbet and Gurney (1983). Let q be the development level of salmon lice such that q increases at a temperature-dependent rate $\gamma_x(T(t)) = \gamma_x(t)$ where $x = P$ or C . Suppose $q = q_P = 0$ at the start of stage P , $q = q_I$ at the transition from P to I , $q = q_C$ at the transition from I to C , and $q = q_A$ at the transition from C to A . Let $\rho(q, t)$ be the density of salmon lice with development level q at time t . Then $M_P(t) = \gamma_P(t)\rho(q_I, t)$, $M_C(t) = \gamma_C(t)\rho(q_A, t)$.

Let $J(q, t)$ be the flux, in the direction of increasing q , of salmon lice with development level q at time t . Then we have the equations (see, e.g., Kot 2001),

$$\frac{\partial \rho(q, t)}{\partial t} = -\frac{\partial J(q, t)}{\partial q} - \mu_P(t)\rho(q, t), \quad q \in [q_P, q_I] \tag{S.11}$$

and,

$$\frac{\partial \rho(q, t)}{\partial t} = -\frac{\partial J(q, t)}{\partial q} - \mu_C(t)\rho(q, t), \quad q \in [q_C, q_A]. \tag{S.12}$$

Since $J(q, t) = \rho(q, t)\gamma_x(t)$, with $x = P, C$, we have

$$\frac{\partial \rho(q, t)}{\partial t} = -\frac{\partial}{\partial q}[\rho(q, t)\gamma_P(t)] - \mu_P(t)\rho(q, t) \quad q \in [q_P, q_I] \tag{S.13}$$

and,

$$\frac{\partial \rho(q, t)}{\partial t} = -\frac{\partial}{\partial q}[\rho(q, t)\gamma_C(t)] - \mu_C(t)\rho(q, t) \quad q \in [q_C, q_A]. \tag{S.14}$$

For the P state, system (S.13) has the boundary condition

$$\rho(q_P, t) = \frac{\eta(t)\epsilon(t)v(t)A(t)}{\gamma_P(t)}.$$

To solve system (S.13) with this boundary condition, we introduce a new variable

$$\xi = h(t) := q_P + \int_0^t \gamma_P(s)ds.$$

Let $h^{-1}(\xi)$ be the inverse function of $h(t)$, and define

$$\hat{\rho}(q, \xi) = \rho(q, h^{-1}(\xi)), \quad \hat{\mu}_P(\xi) = \mu_P(h^{-1}(\xi)), \quad \hat{\gamma}_P(\xi) = \gamma_P(h^{-1}(\xi)).$$

Given (S.13), we then have

$$\frac{\partial \hat{\rho}(q, \xi)}{\partial \xi} = -\frac{\partial \hat{\rho}(q, \xi)}{\partial q} - \frac{\hat{\mu}_P(\xi)}{\hat{\gamma}_P(\xi)} \hat{\rho}(q, \xi). \quad (\text{S.15})$$

This equation is identical in form to the standard von Foerster equation (see Nisbet and Gurney 1982). Let $V(s) = \hat{\rho}(s + q - \xi, s)$. It follows from (S.15) that

$$\frac{dV(s)}{ds} = -\frac{\hat{\mu}_P(s)}{\hat{\gamma}_P(s)} V(s).$$

Since $\xi - (q - q_P) \leq \xi$, we have

$$V(\xi) = V(\xi - (q - q_P)) e^{-\int_{\xi - (q - q_P)}^{\xi} \frac{\hat{\mu}_P(s)}{\hat{\gamma}_P(s)} ds},$$

and hence,

$$\hat{\rho}(q, \xi) = \hat{\rho}(q_P, \xi - q + q_P) e^{-\int_{\xi - q + q_P}^{\xi} \frac{\hat{\mu}_P(s)}{\hat{\gamma}_P(s)} ds}.$$

Define $\tau_P(q, t)$ to be the time taken to grow from development level q_P to level q by salmon lice who arrive at development level q at time t . Since $\frac{dq}{dt} = \gamma_P(t)$ for $q \in [q_I, q_P]$, it follows that

$$q - q_P = \int_{t - \tau_P(q, t)}^t \gamma_P(s) ds, \quad q \in [q_P, q_I], \quad (\text{S.16})$$

and hence,

$$h(t - \tau_P(q, t)) = h(t) - \int_{t - \tau_P(q, t)}^t \gamma_P(s) ds = h(t) - (q - q_P).$$

By the change of variable $s = h(\alpha)$, we then see that

$$\int_{\xi - q + q_P}^{\xi} \frac{\hat{\mu}_P(s)}{\hat{\gamma}_P(s)} ds = \int_{t - \tau_P(q, t)}^t \mu_P(\alpha) d\alpha.$$

It follows that

$$\begin{aligned} \rho(q, t) &= \hat{\rho}(q, h(t)) \\ &= \rho(q_P, t - \tau_P(q, t)) e^{-\int_{t - \tau_P(q, t)}^t \mu_P(\alpha) d\alpha} \\ &= \frac{\eta(t - \tau_P(q, t)) \epsilon(t - \tau_P(q, t)) v(t - \tau_P(q, t)) A(t - \tau_P(q, t))}{\gamma_P(t - \tau_P(q, t))} \phi_P(t). \end{aligned}$$

where $\phi_P(t) = e^{-\int_{t - \tau_P(q, t)}^t \mu_P(\alpha) d\alpha}$. Denote $\tau_P(t) = \tau_P(q_I, t)$, then we have

$$\begin{aligned} \gamma_P(t) \rho(q_I, t) &= \eta(t - \tau_P(t)) \epsilon(t - \tau_P(t)) v(t - \tau_P(t)) A(t - \tau_P(t)) \frac{\gamma_P(t)}{\gamma_P(t - \tau_P(t))} \phi_P(t), \\ &= M_P(t). \end{aligned} \quad (\text{S.17})$$

Substituting equation (S.17) into (S.10), we then have the $\frac{dP(t)}{dt}$ and $\frac{dI(t)}{dt}$ equations in the system (1) in the main text. By similar arguments, we can obtain,

$$M_C(t) = \gamma_C(t) \rho(q_A, t) = \iota f I(t - \tau_C(t)) (1 - \tau'_C(t)) e^{-\int_{t - \tau_C(t)}^t \mu_C(\alpha) d\alpha},$$

which when substituted into (S.10) gives the $\frac{dC(t)}{dt}$ and $\frac{dA(t)}{dt}$ equations in system (1) in the main text.

We note that the maturation rates into the $I(t)$ and $A(t)$ stages ($M_P(t)$ and $M_C(t)$), do not depend on the abundance of the preceding stages ($P(t)$ and $C(t)$). For delay differential equation models, it is not always necessary to specify the dynamics of all stages, for example see Gurney et al. (1980), whereby the model (equation 6 in Gurney et al. 1980) describes the change in only the mature adult fly population. The parameter T_D is the time to reach the mature adult stage from an egg, such that the stage occurring between the egg and the mature adult stage (pupae) has been omitted from the model specification due to the assumption of time delayed maturation. For our model (equations 1), we include the dP/dt and dC/dt equations because we report results related to these quantities, however, the dP/dt and dC/dt equations do not affect the model dynamics.

Letting $q = q_I$ in (S.16) we get,

$$q_I - q_P = \int_{t-\tau_P(t)}^t \gamma_P(s) ds. \quad (\text{S.18})$$

Taking the derivative with respect to t on both sides of (S.18) we obtain,

$$1 - \tau_P'(t) = \frac{\gamma_P(t)}{\gamma_P(t - \tau_P(t))},$$

which is the $\frac{d\tau_P(t)}{dt}$ equation appearing in (2) in the main text. Define $\tau_C(t)$ to be the time taken to grow from development level q_C to level q_A by salmon lice who arrive at development level q_A at time t . We then have,

$$q_A - q_C = \int_{t-\tau_C(t)}^t \gamma_C(s) ds. \quad (\text{S.19})$$

Taking the derivative with respect to t on both sides of (S.19) we have

$$1 - \tau_C'(t) = \frac{\gamma_C(t)}{\gamma_C(t - \tau_C(t))}, \quad (\text{S.20})$$

which is the $\frac{d\tau_C(t)}{dt}$ equation appearing in (2) in the main text. By virtue of (S.18) and (S.19), it easily follows that if $\gamma_x(t)$ is a periodic function, then so is $\tau_x(t)$ with the same period ($x = P$ or C).

S.3 Threshold dynamics

In this section, we study the global dynamics of system (1) and (2). First, we will use the theory recently developed in Zhao (2017) to derive the basic reproduction ratio R_0 . Since the $\frac{dP(t)}{dt}$ and $\frac{dC(t)}{dt}$ equations of system (1) are decoupled from the other equations, it suffices to study the following system:

$$\begin{aligned} \frac{dI(t)}{dt} &= -a_{11}(t)I(t) + a_{12}(t)A(t - \tau_P(t)), \\ \frac{dA(t)}{dt} &= a_{21}(t)I(t - \tau_C(t)) - a_{22}(t)A(t), \end{aligned} \quad (\text{S.21})$$

where $a_{11}(t) = \iota f + \mu_I(t)$, $a_{21}(t) = \frac{1}{2} f \frac{\gamma_C(t)}{\gamma_C(t - \tau_C(t))} \phi_C(t)$, $a_{22}(t) = \mu_A(t)$, and $a_{12}(t) = \eta(t)\epsilon(t)v(t - \tau_P(t)) \frac{\gamma_P(t)}{\gamma_P(t - \tau_P(t))} \phi_P(t)$. Let $\hat{\tau} = \max\{\max_{t \in [0, \omega]} \tau_P(t), \max_{t \in [0, \omega]} \tau_C(t)\}$, $C = C([-\hat{\tau}, 0], \mathbb{R}^2)$, $C^+ = C([-\hat{\tau}, 0], \mathbb{R}_+^2)$. Then (C, C^+) is an ordered Banach space equipped with the maximum norm and the positive cone C^+ . For any given continuous function $v = (v_1, v_2) : [-\hat{\tau}, \sigma] \rightarrow \mathbb{R}^2$ with $\sigma > 0$, we define $v_t \in C$

by

$$v_t(\theta) = (v_1(t + \theta), v_2(t + \theta)), \quad \forall \theta \in [-\hat{\tau}, 0]$$

for any $t \in [0, \sigma)$. Let $F : \mathbb{R} \rightarrow \mathcal{L}(C, \mathbb{R}^2)$ be a map and $V(t)$ be a continuous 2×2 matrix function on \mathbb{R} defined as follows:

$$F(t)\varphi = \begin{bmatrix} a_{12}(t)\varphi_2(-\tau_P(t)) \\ a_{21}(t)\varphi_1(-\tau_C(t)) \end{bmatrix}, \quad V(t) = \begin{bmatrix} a_{11}(t) & 0 \\ 0 & a_{22}(t) \end{bmatrix}.$$

Then the internal evolution of the compartments I and A can be expressed by

$$\frac{du(t)}{dt} = -V(t)u(t).$$

Let $\Phi(t, s), t \geq s$, be the evolution matrix of the above linear system. That is, $\Phi(t, s)$ satisfies

$$\frac{\partial}{\partial t} \Phi(t, s) = -V(t)\Phi(t, s), \quad \forall t \geq s,$$

and

$$\Phi(s, s) = I, \quad \forall s \in \mathbb{R},$$

where I is the 2×2 identity matrix. It then easily follows that

$$\Phi(t, s) = \begin{bmatrix} e^{-\int_s^t a_{11}(r)dr} & 0 \\ 0 & e^{-\int_s^t a_{22}(r)dr} \end{bmatrix}.$$

Let C_ω be the ordered Banach space of all continuous and ω -periodic functions from \mathbb{R} to \mathbb{R}^2 , which is equipped with the maximum norm and the positive cone $C_\omega^+ := \{v \in C_\omega : v(t) \geq 0, \forall t \in \mathbb{R}\}$. Suppose that $v \in C_\omega$ is the initial distribution of copepodid and adult female individuals. Then for any given $s \geq 0$, $F(t-s)v_{t-s}$ is the distribution of offspring (copepodids and adult females) at time $t-s$, which is produced by the individuals who were introduced over the time interval $[t-s-\hat{\tau}, t-s]$. Then $\Phi(t, t-s)F(t-s)v_{t-s}$ is the distribution of those individuals who newly entered the copepodid or adult female compartments at time $t-s$ and remain in the compartments at time t . It follows that

$$\int_0^\infty \Phi(t, t-s)F(t-s)v_{t-s}ds = \int_0^\infty \Phi(t, t-s)F(t-s)v(t-s+\cdot)ds$$

is the cumulative distribution of new copepodids and adult females at time t produced by all the copepodids and adult females introduced at all times prior to t .

Define a linear operator $L : C_\omega \rightarrow C_\omega$ by

$$[Lv](t) = \int_0^\infty \Phi(t, t-s)F(t-s)v(t-s+\cdot)ds, \quad \forall t \in \mathbb{R}, \quad v \in C_\omega.$$

Following Zhao (2017), we define $R_0 = r(L)$, the spectral radius of L . Let $\hat{P}(t)$ be the solution maps of system (S.21) on C , that is, $\hat{P}(t)\varphi = y_t(\varphi), t \geq 0$, where $y(t, \varphi)$ is the unique solution of (S.21) with $y_0 = \varphi \in C$. Then $\hat{P} := \hat{P}(\omega)$ is the Poincaré map associated with linear system (S.21). Let $r(\hat{P})$ be the spectral radius of \hat{P} . In light of Zhao (2017, Theorem 2.1), we have the following observation.

Lemma 1 $R_0 - 1$ has the same sign as $r(\hat{P}) - 1$.

By Hale (1993, Theorem 6.1.1) and Smith (1995, Theorem 5.2.1), we obtain the following result for linear system (S.21).

Lemma 2 For any $\varphi \in C^+$, system (S.21) has a unique solution $y(t, \varphi)$ with $y_0 = \varphi$, and $y(t, \varphi) \geq 0$ for all $t \geq 0$.

Let

$$\Omega := C([- \tau_C(0), 0], \mathbb{R}_+) \times C([- \tau_P(0), 0], \mathbb{R}_+).$$

Then we further have the following result.

Lemma 3 For any $\varphi \in \Omega$, system (S.21) has a unique solution $z(t, \varphi)$ with $z_0 = \varphi$, and $z_t(\varphi) := (z_{1t}(\varphi), z_{2t}(\varphi)) \in \Omega$ for all $t \geq 0$.

Proof Let $\bar{\tau} = \min\{\min_{t \in [0, \omega]} \tau_P(t), \min_{t \in [0, \omega]} \tau_C(t)\}$. For any $t \in [0, \bar{\tau}]$, since $t - \tau_P(t)$ and $t - \tau_C(t)$ are strictly increasing in t , we have

$$- \tau_x(0) = 0 - \tau_x(0) \leq t - \tau_x(t) \leq \bar{\tau} - \tau_x(\bar{\tau}) \leq \bar{\tau} - \bar{\tau} = 0, \quad x = P, C,$$

and hence,

$$z_1(t - \tau_C(t)) = \varphi_1(t - \tau_C(t)), z_2(t - \tau_P(t)) = \varphi_2(t - \tau_P(t)).$$

Therefore, we have the following ordinary differential equations for $t \in [0, \bar{\tau}]$:

$$\begin{aligned} \frac{dz_1(t)}{dt} &= \eta(t - \tau_P(t))\epsilon(t - \tau_P(t))v(t - \tau_P(t))\varphi_2(t - \tau_P(t))(1 - \tau'_P(t))e^{-\int_{t-\tau_P(t)}^t \mu_P(s)ds} - (\iota f + \mu_I(t))z_1(t), \\ \frac{dz_2(t)}{dt} &= \frac{1}{2}\iota f\varphi_1(t - \tau_C(t))(1 - \tau'_C(t))e^{-\int_{t-\tau_C(t)}^t \mu_C(s)ds} - \mu_A(t)z_2(t). \end{aligned}$$

Given $\varphi \in \Omega$, the solution $(z_1(t), z_2(t))$ of the above system exists for $t \in [0, \bar{\tau}]$. In other words, we have obtained values of $\psi_1(\theta) = z_1(\theta)$ for $\theta \in [-\tau_C(0), \bar{\tau}]$ and $\psi_2(\theta) = z_2(\theta)$ for $\theta \in [-\tau_P(0), \bar{\tau}]$.

For any $t \in [\bar{\tau}, 2\bar{\tau}]$, we have

$$- \tau_x(0) = 0 - \tau_x(0) \leq \bar{\tau} - \tau_x(\bar{\tau}) \leq t - \tau_x(t) \leq 2\bar{\tau} - \tau_x(2\bar{\tau}) \leq 2\bar{\tau} - \bar{\tau} = \bar{\tau}, \quad x = P, C,$$

and hence, $z_1(t - \tau_C(t)) = \psi_1(t - \tau_C(t))$, $z_2(t - \tau_P(t)) = \psi_2(t - \tau_P(t))$. Solving the following system of ordinary differential equations for $t \in [\bar{\tau}, 2\bar{\tau}]$ with $z_1(\bar{\tau}) = \psi_1(\bar{\tau})$ and $z_2(\bar{\tau}) = \psi_2(\bar{\tau})$:

$$\begin{aligned} \frac{dz_1(t)}{dt} &= \eta(t - \tau_P(t))\epsilon(t - \tau_P(t))v(t - \tau_P(t))\psi_2(t - \tau_P(t))(1 - \tau'_P(t))e^{-\int_{t-\tau_P(t)}^t \mu_P(s)ds} - (\iota f + \mu_I(t))z_1(t), \\ \frac{dz_2(t)}{dt} &= \frac{1}{2}\iota f\psi_1(t - \tau_C(t))(1 - \tau'_C(t))e^{-\int_{t-\tau_C(t)}^t \mu_C(s)ds} - \mu_A(t)z_2(t), \end{aligned}$$

we then get the solution $(z_1(t), z_2(t))$ on $[\bar{\tau}, 2\bar{\tau}]$. Repeating this procedure for $t \in [2\bar{\tau}, 3\bar{\tau}]$, $[3\bar{\tau}, 4\bar{\tau}]$, ..., it then follows that for any $\varphi \in \Omega$, system (S.21) has a unique solution $z(t, \varphi)$ with $z_0 = \varphi$ and $z_t(\varphi) = (z_{1t}(\varphi), z_{2t}(\varphi)) \in \Omega$ for all $t \geq 0$.

Remark 1 By the uniqueness of solutions in Lemmas 2 and 3, it follows that for any $\psi \in C_+$ and $\phi \in \Omega$ with $\psi_1(\theta) = \phi_1(\theta)$ for all $\theta \in [-\tau_C(0), 0]$ and $\psi_2(\theta) = \phi_2(\theta)$ for all $\theta \in [-\tau_P(0), 0]$, we have $y(t, \psi) = z(t, \phi)$, $\forall t \geq 0$, where $y(t, \psi)$ and $z(t, \phi)$ are solutions of system (S.21) satisfying $y_0 = \psi$ and $z_0 = \phi$, respectively.

Let $P(t)$ be the solution maps of system (S.21) on Ω , that is, $P(t)\varphi = z_t(\varphi)$, $t \geq 0$, where $z(t, \varphi)$ is the unique solution of system (S.21) with $z_0 = \varphi \in \Omega$. By the arguments similar to those in Lou and Zhao (2017, Lemma 3.5), we have the following result.

Lemma 4 $P(t) : \Omega \rightarrow \Omega$ is an ω -periodic semiflow in the sense that (i) $P(0) = I$; (ii) $P(t + \omega) = P(t) \circ P(\omega)$, $\forall t \geq 0$; (iii) $P(t)\varphi$ is continuous in $(t, \varphi) \in [0, \infty) \times \Omega$.

Let P be the Poincaré map of the linear system (S.21) on the space Ω , and $r(P)$ be its spectral radius. Then we have the following threshold result for system (S.21).

Lemma 5 *The following statements are valid:*

(i) If $r(P) \leq 1$, then $\lim_{t \rightarrow \infty} (I(t, \varphi), A(t, \varphi)) = (0, 0)$ for any $\varphi \in \Omega$.

(ii) If $r(P) > 1$, then $\lim_{t \rightarrow \infty} (I(t, \varphi), A(t, \varphi)) = (\infty, \infty)$ for any $\varphi \in \Omega \setminus \{0\}$.

Proof For any given $\varphi, \psi \in \Omega$ with $\varphi \geq \psi$, let $\bar{u}(t) = u(t, \varphi)$ and $u(t) = u(t, \psi)$ be the unique solutions of system (S.21) with $u_0 = \varphi$ and $u_0 = \psi$, respectively. Let $\bar{\tau} = \min\{\min_{t \in [0, \omega]} \tau_P(t), \min_{t \in [0, \omega]} \tau_C(t)\}$.

Since for any $t \in [0, \bar{\tau}]$,

$$-\tau_x(0) = 0 - \tau_x(0) \leq t - \tau_x(t) \leq \bar{\tau} - \tau_x(\bar{\tau}) \leq \bar{\tau} - \bar{\tau} = 0, \quad x = P, C,$$

we have $\bar{u}_1(t - \tau_C(t)) = \varphi_1(t - \tau_C(t))$, $u_1(t - \tau_C(t)) = \psi_1(t - \tau_C(t))$, $\bar{u}_2(t - \tau_P(t)) = \varphi_2(t - \tau_P(t))$ and $u_2(t - \tau_P(t)) = \psi_2(t - \tau_P(t))$ for all $t \in [0, \bar{\tau}]$, and hence, $\bar{u}_1(t - \tau_C(t)) \geq u_1(t - \tau_C(t))$ and $\bar{u}_2(t - \tau_P(t)) \geq u_2(t - \tau_P(t))$ for all $t \in [0, \bar{\tau}]$. In view of $\bar{u}(0) = \varphi(0) \geq \psi(0) = u(0)$, the comparison theorem for cooperative ordinary differential systems implies that $\bar{u}(t) \geq u(t)$ for all $t \in [0, \bar{\tau}]$. Repeating this procedure for $t \in [\bar{\tau}, 2\bar{\tau}]$, $[2\bar{\tau}, 3\bar{\tau}]$, ..., it follows that $u(t, \varphi) \geq u(t, \psi)$ for all $t \in [0, \infty)$. This implies that $P(t) : \Omega \rightarrow \Omega$ is monotone for each $t \geq 0$. Next we show that the solution map $P(t) : \Omega \rightarrow \Omega$ is eventually strongly monotone. Let $\varphi, \psi \in \Omega$ satisfy $\varphi > \psi$. Denote $u(t, \varphi) = (\bar{y}_1(t), \bar{y}_2(t))$ and $u(t, \psi) = (y_1(t), y_2(t))$. Without loss of generality, we assume that $\varphi_1 > \psi_1$.

Since $1 - \tau'_C(t) > 0$, there exists a unique solution to the equation $t - \tau_C(t) = 0$. Denote the unique solution of $t - \tau_C(t) = 0$ as \bar{t} , i.e., $\bar{t} - \tau_C(\bar{t}) = 0$.

Claim 1. There exists $t_0 \in [0, \bar{t}]$ such that $\bar{y}_2(t) > y_2(t)$, $\forall t \geq t_0$.

We first prove that $\bar{y}_2(t_0) > y_2(t_0)$ for some $t_0 \in [0, \bar{t}]$. Otherwise, we have $\bar{y}_2(t) = y_2(t)$, $\forall t \in [0, \bar{t}]$, and hence, $\frac{d\bar{y}_2(t)}{dt} = \frac{dy_2(t)}{dt}$, $\forall t \in (0, \bar{t})$. Thus, we have

$$\frac{1}{2} \iota f(1 - \tau'_C(t)) e^{-\int_{t-\tau_C(t)}^t \mu_C(s) ds} [\bar{y}_1(t - \tau_C(t)) - y_1(t - \tau_C(t))] = 0, \forall t \in [0, \bar{t}]. \quad (\text{S.22})$$

It follows that $\bar{y}_1(t - \tau_C(t)) = y_1(t - \tau_C(t))$ for all $t \in [0, \bar{t}]$, that is, $\varphi_1(\theta) = \psi_1(\theta)$ for all $\theta \in [-\tau_C(0), 0]$, which contradicts the assumption that $\varphi_1 > \psi_1$.

Let

$$g_1(t, y) := \frac{1}{2} \iota f(1 - \tau'_C(t)) e^{-\int_{t-\tau_C(t)}^t \mu_C(s) ds} y_1(t - \tau_C(t)) - \mu_A(t)y.$$

Since

$$\begin{aligned} \frac{d\bar{y}_2(t)}{dt} &= \frac{1}{2} \iota f(1 - \tau'_C(t)) e^{-\int_{t-\tau_C(t)}^t \mu_C(s) ds} \bar{y}_1(t - \tau_C(t)) - \mu_A(t)\bar{y}_2(t) \\ &\geq \frac{1}{2} \iota f(1 - \tau'_C(t)) e^{-\int_{t-\tau_C(t)}^t \mu_C(s) ds} y_1(t - \tau_C(t)) - \mu_A(t)\bar{y}_2(t) \\ &= g_1(t, \bar{y}_2(t)), \end{aligned}$$

we have

$$\frac{d\bar{y}_2(t)}{dt} - g_1(t, \bar{y}_2(t)) \geq 0 = \frac{dy_2(t)}{dt} - g_1(t, y_2(t)), \quad \forall t \geq t_0.$$

Since $\bar{y}_2(t_0) > y_2(t_0)$, the comparison theorem for ordinary differential equations (Theorem 4, Walter 1997) implies that $\bar{y}_2(t) > y_2(t), \forall t \geq t_0$.

Denote the unique solution to $t - \tau_P(t) = t_0$ as \tilde{t} .

Claim 2. $\bar{y}_1(t) > y_1(t), \forall t > \tilde{t}$.

Let

$$g_2(t, y) := \eta(t - \tau_P(t))\epsilon(t - \tau_P(t))v(t - \tau_P(t))(1 - \tau_P'(t))e^{-\int_{t-\tau_P(t)}^t \mu_P(s)ds} y_2(t - \tau_P(t)) - (\iota f + \mu_I(t))y.$$

Then we have

$$\begin{aligned} \frac{d\bar{y}_1(t)}{dt} &= \eta(t - \tau_P(t))\epsilon(t - \tau_P(t))v(t - \tau_P(t))(1 - \tau_P'(t))e^{-\int_{t-\tau_P(t)}^t \mu_P(s)ds} \bar{y}_2(t - \tau_P(t)) - (\iota f + \mu_I(t))\bar{y}_1(t) \\ &> \eta(t - \tau_P(t))\epsilon(t - \tau_P(t))v(t - \tau_P(t))(1 - \tau_P'(t))e^{-\int_{t-\tau_P(t)}^t \mu_P(s)ds} y_2(t - \tau_P(t)) - (\iota f + \mu_I(t))\bar{y}_1(t) \\ &= g_2(t, \bar{y}_1(t)), \quad \forall t \geq \tilde{t}, \end{aligned}$$

and hence,

$$\frac{d\bar{y}_1(t)}{dt} - g_2(t, \bar{y}_1(t)) > 0 = \frac{dy_1(t)}{dt} - g_2(t, y_1(t)), \quad \forall t \geq \tilde{t}.$$

Since $\bar{y}_1(\tilde{t}) \geq y_1(\tilde{t})$, it follows from Walter (1997, Theorem 4) that $\bar{y}_1(t) > y_1(t), \forall t > \tilde{t}$.

In view of Claims 1 and 2, we obtain

$$(\bar{y}_1(t), \bar{y}_2(t)) \gg (y_1(t), y_2(t)), \quad \forall t > t^* := \max\{\bar{t}, \tilde{t}\}.$$

It follows that

$$(\bar{y}_{1t}, \bar{y}_{2t}) \gg (y_{1t}, y_{2t}), \quad \forall t > t^* + \tau_P(0) + \tau_C(0).$$

This shows that $P(t) : \Omega \rightarrow \Omega$ is strongly monotone for any $t > t^* + \tau_P(0) + \tau_C(0)$. It follows from Hale (1993, Theorem 3.6.1) that the linear operator $P(t)$ is compact on Ω . Choose an integer n_0 such that $n_0\omega > t^* + \tau_P(0) + \tau_C(0)$. Since $P^{n_0} = P(n_0\omega)$, Liang and Zhao (2007, Lemma 3.1) implies that $r(P)$ is a simple eigenvalue of P having a strongly positive eigenvector, and the modulus of any other eigenvalue is less than $r(P)$. It then follows from Wang and Zhao (2017, Lemma 1) that there is a positive ω -periodic function $\bar{v}(t) = (\bar{v}_1(t), \bar{v}_2(t))$ such that $v^*(t) = e^{\frac{\ln r(P)}{\omega}t} \bar{v}(t)$ is a positive solution of system (S.21).

In the case where $r(P) < 1$, we have $\lim_{t \rightarrow \infty} v^*(t) = 0$. For any $\varphi \in \Omega$, choose a sufficiently large number $K > 0$ such that $\varphi \leq K v_0^*$. Then by the comparison theorem, we have

$$(I(t, \varphi), A(t, \varphi)) \leq K v^*(t), \quad \forall t \geq 0.$$

Hence, $\lim_{t \rightarrow \infty} I(t, \varphi) = \lim_{t \rightarrow \infty} A(t, \varphi) = 0$. This proves statement (i).

In the case where $r(P) > 1$, we have $\lim_{t \rightarrow \infty} v^*(t) = \infty$. For any $\varphi \in \Omega \setminus \{0\}$, we have $u_t(\varphi) \gg 0$ for all $t > t^* + \tau_P(0) + \tau_C(0)$. Without loss of generality, we assume that $\varphi \gg 0$. Then we can choose a sufficiently small real number $\delta > 0$ such that $\varphi_1(\theta) \geq \delta v_1^*(\theta)$, $\theta \in [-\tau_C(0), 0]$, $\varphi_2(\theta) \geq \delta v_2^*(\theta)$, $\theta \in [-\tau_P(0), 0]$. Then by the comparison theorem, we have

$$(I(t, \varphi), A(t, \varphi)) \geq \delta v^*(t), \quad \forall t \geq 0.$$

Hence, $\lim_{t \rightarrow \infty} (I(t, \varphi), A(t, \varphi)) = (\infty, \infty)$. This proves statement (ii).

By the same arguments as in Lou and Zhao (2017, Lemma 3.8), we have $r(P) = r(\hat{P})$. Combining Lemmas 1 and 5, we have the following result on the global dynamics of system (S.21).

Theorem 2 *The following statements are valid:*

- (i) *If $R_0 < 1$, then the extinction equilibrium $(0, 0)$ is globally attractive for system (S.21) in Ω ;*
- (ii) *If $R_0 > 1$, then all nontrivial solutions of system (S.21) go to infinity eventually.*

In the rest of this section, we derive the dynamics for the variables $P(t)$ and $C(t)$ in system (1). Under the compatibility condition

$$\begin{aligned} P(0) &= \int_{t-\tau_P(0)}^0 \eta(\xi)\epsilon(\xi)v(\xi)A(\xi)e^{-\int_{\xi}^0 \mu_P(s)ds} d\xi, \\ C(0) &= \int_{t-\tau_C(0)}^0 \iota f I(\xi)e^{-\int_{\xi}^0 \mu_C(s)ds} d\xi, \end{aligned} \tag{S.23}$$

we can solve $P(t)$ and $C(t)$ as

$$\begin{aligned} P(t) &= \int_{t-\tau_P(t)}^t \eta(\xi)\epsilon(\xi)v(\xi)A(\xi)e^{-\int_{\xi}^t \mu_P(s)ds} d\xi, \\ C(t) &= \int_{t-\tau_C(t)}^t \iota f I(\xi)e^{-\int_{\xi}^t \mu_C(s)ds} d\xi. \end{aligned} \tag{S.24}$$

In the case where $R_0 < 1$, we have $\lim_{t \rightarrow \infty} A(t) = \lim_{t \rightarrow \infty} I(t) = 0$, and hence, the expression (S.24) implies that $\lim_{t \rightarrow \infty} P(t) = \lim_{t \rightarrow \infty} C(t) = 0$.

In the case where $R_0 > 1$, we obtain $\lim_{t \rightarrow \infty} A(t) = \lim_{t \rightarrow \infty} I(t) = +\infty$. It then follows from (S.24) that $\lim_{t \rightarrow \infty} P(t) = \lim_{t \rightarrow \infty} C(t) = +\infty$. Consequently, using these arguments combined with Lemma 1, we have the result stated in the main text (Theorem 1) describing the global dynamics of system (1) and (2).

S.4 Numerical methods

The system of equations (1) and (2), was solved using the `dde()` and `pastvalue()` functions in the *PBSddesolve* package for R (Couture-Beil et al., 2016). This solver for delay differential equations is based on Simon Wood's *sol95* program (Wood, 1999) written in C/C++ and using an adaptively stepped embedded RK2(3) scheme with cubic hermite interpolation of the lagged variables.

Figure 3 in the main text assumes $A(0) = f$ and $P(0) = I(0) = C(0) = 0$ and Figure 4 assumes $A(0) = P(0) = I(0) = C(0) = f$. For Figures 3 and 4, we assumed the initial history, $t < 0$, for each variable was equal to their respective values at $t = 0$. The initial values of the time delays were calculated by numerically solving equation (S.18) with $q_I - q_P = 1$ and equation (S.19) with $q_A - q_C = 1$. To numerically evaluate the integral we used R's `integrate()` function and to find the value of the integral equal to 1 we used the `uniroot()` function.

To find the spectral radius of the Poincaré map, $r(\hat{P})$, we used the method described in Liang et al. (2017, Lemma 2.5), which is similar to the Power method (Wikipedia, 2018), but specifically developed for delay differential equations. This algorithm involves numerically solving,

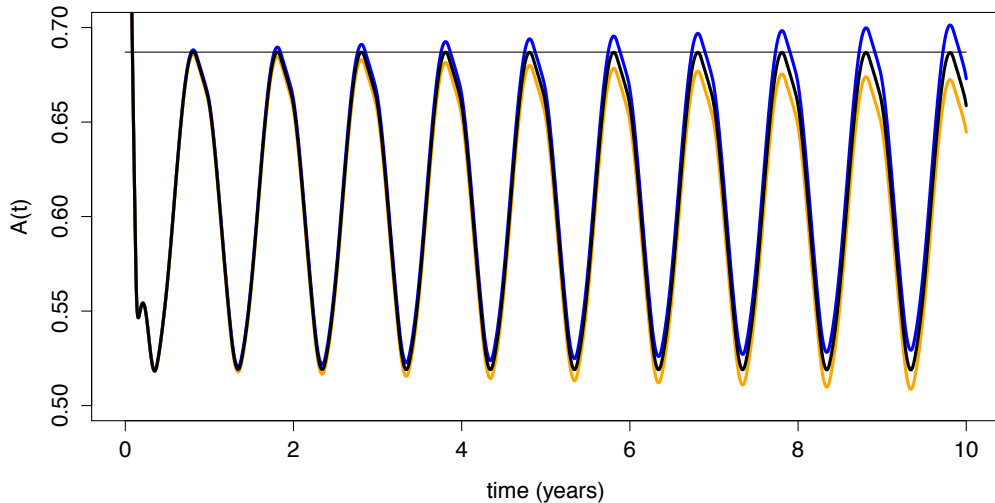


Fig. S.3 Numerical verification of f_{crit} as the threshold for population growth. Numerical solutions to the system (1) and (2) parameterized for the BCB site with $f = f_{crit}$ (black), $f = f_{crit} - 100$ (orange), and $f = f_{crit} + 100$ (blue) confirm that f_{crit} is the threshold value of population growth. A horizontal line is shown at $A(t) = 0.687$ for reference.

$$\begin{aligned}
 \frac{dI(t)}{dt} &= -a_{11}(t)I(t) + \frac{a_{12}(t)}{\lambda}A(t - \tau_P(t)), \\
 \frac{dA(t)}{dt} &= \frac{a_{21}(t)}{\lambda}I(t - \tau_C(t)) - a_{22}(t)A(t), \\
 \frac{d\tau_P(t)}{dt} &= 1 - \frac{\gamma_P(t)}{\gamma_P(t - \tau_P(t))}, \\
 \frac{d\tau_C(t)}{dt} &= 1 - \frac{\gamma_C(t)}{\gamma_C(t - \tau_C(t))},
 \end{aligned} \tag{S.25}$$

where $a_{11}(t) = \iota f + \mu_I(t)$, $a_{21}(t) = \frac{1}{2}f \frac{\gamma_C(t)}{\gamma_C(t - \tau_C(t))} \phi_C(t)$, $a_{22}(t) = \mu_A(t)$, and $a_{12}(t) = \eta(t)\epsilon(t)v(t - \tau_P(t)) \frac{\gamma_P(t)}{\gamma_P(t - \tau_P(t))} \phi_P(t)$. The system (S.21) is the same as the system of equations (1) from the main text except that $\frac{dP(t)}{dt}$ and $\frac{dC(t)}{dt}$ are removed because the two equations are decoupled from system (1) (see Section S.3), and the $a_{12}(t)$ and $a_{21}(t)$ terms are divided by λ to calculate R_0 as detailed in equation (2.11) of Zhao (2017).

The net reproductive ratio, R_0 , is the value of λ such that $r(\hat{P}) = 1$, and we solved for this value using the `uniroot()` function. The Floquet exponent was calculated as $\mu = \log(M)/\omega$ when λ was set to 1. The critical stocking density was calculated as the value of f such that $\mu = 0$ and was implemented using the `uniroot()` function. Figure S.3 shows the dynamics of (1) for f_{crit} (black), $f_{crit} + 100$ (blue), and $f_{crit} - 100$ (orange).

S.5 The follow-up treatment window in seasonal environments

For a sea louse that became an adult female at time \tilde{t} , we back-calculate the time when the chalimus stage was reached, $t_C(\tilde{t})$, and when hatching occurred (i.e., the nauplius stage was first reached), $t_P(\tilde{t})$, as:

$$t_P(\tilde{t}) = \tau_P(\tilde{t} - \tau_C(\tilde{t}) - 10), \quad (\text{S.26})$$

$$t_C(\tilde{t}) = \tilde{t} - \tau_C(\tilde{t}), \quad (\text{S.27})$$

where $\tilde{t} - \tau_C(\tilde{t}) - 10$ is the time when the copepodid stage was reached for a louse that became an adult female at \tilde{t} . In Figure 4, we plot the time of an initial treatment, t_0 , on the x-axis. To plot the start of the follow-up treatment window in Figure 4, we identify salmon lice that hatched at the time of the initial treatment, $t_0 = t_P(\tilde{t})$, and plot the corresponding time to becoming a chalimus, $T_1 = t_C(\tilde{t}) - t_P(\tilde{t})$ where the subtraction is to calculate the number of days to reach the chalimus stage, since $t_C(\tilde{t})$ refers to time (i.e., $t_C(\tilde{t}) = 365$ means the chalimus stage was reached on January 1st of year 2). To plot the end of the treatment window, we identify salmon lice that just became chalimi when the initial treatment occurred, $t_0 = t_C(\tilde{t})$ and plot the time to becoming an adult female, $T_2 = \tilde{t} - t_C(\tilde{t})$. As for the constant temperature case, the treatment window exists for all sites we considered because T_1 is always less than T_2 .

References

- Boxaspen, K. and T. Naess. 2000. Development of eggs and the planktonic stages of salmon lice (*Lepeophtheirus salmonis*) at low temperatures. *Contrib Zool* 69:51-55.
- Bjørn, P.A., and B. Finstad. 1998. The development of salmon lice (*Lepeophtheirus salmonis*) on artificially infected post smolts of sea trout (*Salmo trutta*). *Can J Zool* 76: 970-977.
- Bravo, S. 2003. Salmon lice in Chilean salmon farms. *Bull Eur Ass Fish Pathol* 23(4): 197-200.
- Bravo, S., Pozo, V., and M. T. Sliva. 2008. The tolerance of *Caligus rogercresseyi* to salinity reduced in southern Chile. *Bull Eur Ass Fish Pathol* 28(5): 198-206.
- Bravo, S. 2010. The reproductive output of *Caligus rogercresseyi* under controlled conditions. *Experimental Parasitology* 125: 51-54.
- Brewer-Dalton, K., Page, F.H., Chandler, P. and A. Ratsimandresy. 2015. Oceanographic conditions of salmon farming areas with attention to those factors that may influence the biology and ecology of salmon lice, *Lepeophtheirus salmonis* and *Caligus* spp., and their control. DFO Can Sci Advis Sec Res Doc. 2014/048. 47pp.
- Bricknell, I. R., Dalesman, S. J., O’Shea, B., Pert, C. C., and J. A. Mordue Luntz. 2006. Effect of environmental salinity on salmon lice *Lepeophtheirus salmonis* settlement success. *Disease of Aquatic Organisms* 71: 201-212.
- Connors, B. M., Juarez-Colunga, E., and L. M. Dill. 2008. Effects of varying salinities on *Lepeophtheirus salmonis* survival on juvenile pink and chum salmon. *J Fish Biol* 72: 1825-1830.
- Costello, M. J. 2006. Ecology of sea lice parasitic on farmed and wild fish. *Trends in Parasitology* 22(10): 475-483.
- Couture-Beil, A., Schnute, J.T., Haigh, R. Wood, S. N., Cairns, B.J., and N. Boers. 2016. PBSddesolve: Solver for delay differential equations. <https://github.com/pbs-software/pbs-ddesolve>.

- Dabrowski, T., K. Lyons, C. Cusack, G. Casal, A. Berry, and G. D. Nolan. 2016. Ocean modelling for aquaculture and fisheries in Irish waters. *Ocean Sci.* 12: 101-116.
- Department of Fisheries and Oceans. 2016. State of Knowledge of the Oceanography and Water Exchange on the South Coast of Newfoundland to Support the Development of Bay Management Areas for Finfish Aquaculture. DFO Can. Sci. Advis. Sec. Sci. Advis. Rep. 2016/039.
- Finstad, B., P. A. Bjørn, A. Grimnes, and N. A. Hvidsten. 2001. Laboratory and field investigations of salmon lice (*Lepeophtheirus salmonis* (Krøyer)) infestation on Atlantic salmon (*Salmo salar* L.) post-smolts. *Aquaculture Research* 31(11): 795-803.
- González, L. and J. Carvajal. 2003. Life cycle of *Caligus rogercresseyi* (Copepoda: Caligidae) parasite of Chilean reared salmonids. *Aquaculture* 220: 101-117.
- Grimnes, A. and P. J. Jakobsen. 1996. The physiological effects of salmon lice infection on post-smolt of Atlantic salmon. *J Fish Biol* 48: 1179-1194.
- Groner, M.L., McEwan, G.F., Rees, E.E., Gettinby, G. and C.W. Revie. 2016. Quantifying the influence of salinity and temperature on the population dynamics of a marine ectoparasite. *Can J Fish Aquat Sci* 73: 1-11.
- Gurney, W. S. C., S. P. Blythe, and R. M. Nisbet. 1980. Nicholson's blowflies revisited. *Nature* 287: 17-21.
- Hale, J. K., and S. M. Verduyn Lunel. 1993. *Introduction to Functional Differential Equations*. Springer, New York.
- Heutch, P. A., Nordhagen, J. R., and T. A. Schram. 2000. Egg production in the salmon louse [*Lepeophtheirus salmonis* (Krøyer)] in relation to origin and water temperature, *Aquac Res* 31: 805-814.
- Johannessen, A. 1978. Early stages of *Lepeophtheirus salmonis* (Copepoda, Caligidae). *Sarsia* 63: 169-176.
- Johnson, S. C. and L. J. Albright. 1991. Development, growth, and survival of *Lepeophtheirus salmonis* (Copepoda: Caligidae) under laboratory conditions. *J Mar Biol Assoc U.K.* 71: 425-436.
- Kot, M. 2001. *Elements of Mathematical Ecology*, Cambridge University Press, Cambridge.
- Liang, X., and X.-Q. Zhao. 2017. Asymptotic speeds of spread and traveling waves for monotone semiflows with applications. *Comm Pure Appl Math* 60: 1-40.
- Liang, X., Zhang, L., and X.-Q. Zhao. 2017. Basic reproduction ratios for periodic abstract functional differential equations (with application to a spatial model for Lyme disease). *J. Dynam Differential Equations* doi: 10.1007/s10884-017-9601-7.
- Ljungfeldt, L. E. R., M. Quintela, F. Besnier, F. Nilsen, and K. A. Glover. 2017. A pedigree-based experiment reveals variation in salinity and thermal tolerance in salmon louse, *Lepeophtheirus salmonis*. *Evolutionary Applications* 10(10): 1007-1019.
- Landsberg, J. H., G. K. Vermeer, S. A. Richards, and N. Perry. 1991. Control of the parasitic copepod *Caligus elongatus* on pond-reared red drum. *Journal of Aquatic Animal Health* 3: 206-209.
- Lou, Y. and X.-Q. Zhao. 2017. A theoretical approach to understanding population dynamics with seasonal developmental durations. *J. Nonlinear Science* 27: 573-603.
- Marty, G.D., Saksida, S.M., and T.J. Quinn II. 2010. Relationship of farm salmon, salmon lice, and wild salmon populations. *Proc Natl Acad Sci USA.* 107(52): 22599-22604.

- Montory, J. A., Cumillaf, J. P., Cubillos, V. M., Paschke, K., Urbina, M. A. and P. Bebauer. 2018 Early development of the ectoparasite *Caligus rogercressyi* under combined temperature and salinity gradients. *Aquaculture* 486: 68-74.
- Nisbet, R. M. and W. S. Gurney. 1982. *Modelling Fluctuating Populations*. The Blackburn Press, New Jersey.
- Nisbet, R. M. and W. S. Gurney. 1983. The systematic formulation of population models for insects with dynamically varying instar duration. *Theoret Pop Biol* 23: 114-135.
- Rittenhouse, M. A., Revie, C. W., and A. Hurford. 2016. A model for salmon lice (*Lepeophtheirus salmonis*) dynamics in a seasonally changing environment. *Epidemics* 16: 8-16.
- Samsing, F., Oppedal, F., Dalvin, S., Johnsen, I., Vøegseth, T. and T. Dempster. 2016. Salmon lice (*Lepeophtheirus salmonis*) development times, body size, and reproductive outputs follow universal models of temperature dependence. *Can J Fish Aquat Sci* 731: 1841-1851.
- Skern-Mauritzen, R., O. Torrissen, and K. A. Glover. 2014. Pacific and Atlantic *Lepeophtheirus salmonis* (Kroyer, 1838) are allopatric subspecies: *Lepeophtheirus salmonis salmonis* and *L. salmonis oncorhynchi* subspecies novo. *BMC Genetics* 15: 32.
- Smith, H. L. 1995. *Monotone Dynamical Systems: An Introduction to the Theory of Competitive and Cooperative Systems*, Mathematical Surveys and Monographs 41., American Mathematical Society, Providence.
- Stien, A., Bjorn, P. A., Heuch, P. A., and D. A. Elston. 2005. Population dynamics of salmon lice *Lepeophtheirus salmonis* on Atlantic salmon and sea trout. *Mar Ecol Prog Ser* 290: 263-275.
- Tucker, C. S., Norman, R., Shinn A.P., Bron, J.E., Sommerville, C., and R. Wootten. 2002. A single cohort time delay model of the life-cycle of the salmon louse *Lepeophtheirus salmonis* on Atlantic salmon *Salmo salar*. *Fish Pathol* 37: 107-118.
- Walter, W. 1997. On strongly monotone flows. *ANNALES POLONICI MATHEMATICI* LXVI 269-274.
- Wikipedia. 2018. Power iteration. https://en.wikipedia.org/wiki/Power_iteration
- Wood, S.N. 1999. *Solv95: a numerical solver for systems of delay differential equations with switches*. Saint Andrews, UK. 10pp.
- Wootten, R., Smith, J.W., and E. A. Needham. 1982. Aspects of the biology of the parasitic copepods *Lepeophtheirus salmonis* and *Caligus elongatus* on farmed salmonids, and their treatment. *Proc R Soc Edinb B* 81:185-197.
- Zhao, X.-Q., Basic reproduction ratios for periodic compartmental models with time delay, *J Dynam Differential Equations*, 29, 67-82 (2017).